



High Pressure Research

An International Journal

ISSN: 0895-7959 (Print) 1477-2299 (Online) Journal homepage: <http://www.tandfonline.com/loi/ghpr20>

Pressure and temperature dependence of the structure of liquid Sn up to 5.3 GPa and 1373 K

Daijo Ikuta, Yoshio Kono & Guoyin Shen

To cite this article: Daijo Ikuta, Yoshio Kono & Guoyin Shen (2016): Pressure and temperature dependence of the structure of liquid Sn up to 5.3 GPa and 1373 K, High Pressure Research, DOI: [10.1080/08957959.2016.1185520](https://doi.org/10.1080/08957959.2016.1185520)

To link to this article: <http://dx.doi.org/10.1080/08957959.2016.1185520>



Published online: 19 May 2016.



Submit your article to this journal [↗](#)



Article views: 14



View related articles [↗](#)



View Crossmark data [↗](#)

Full Terms & Conditions of access and use can be found at
<http://www.tandfonline.com/action/journalInformation?journalCode=ghpr20>

Pressure and temperature dependence of the structure of liquid Sn up to 5.3 GPa and 1373 K

Daijo Ikuta, Yoshio Kono and Guoyin Shen

High Pressure Collaborative Access Team, Geophysical Laboratory, Carnegie Institution of Washington, Argonne, IL, USA

ABSTRACT

Pressure and temperature dependence of the structure of liquid Sn has been measured up to 5.3 GPa and 1373 K using multi-angle energy-dispersive X-ray diffraction in Paris–Edinburgh cell. Under nearly isobar condition at ~ 1 GPa, liquid Sn displays a normal behavior with gradual structural changes with temperature up to 1373 K. Under isothermal compressions at 850 and 1373 K, however, the structure factors of liquid Sn both show a turn-over at ~ 3 GPa in the height of the first diffraction peak. According to the hard sphere cluster model, the structure of liquid Sn may be viewed as two different types of clusters. Below ~ 3 GPa, it is shown that the packing fraction of the dominant cluster (occupying ~ 0.94 fraction) changes with compression, while above ~ 3 GPa, the packing fractions and the hard sphere diameters of both clusters start to influence the structure, causing significant changes with increasing pressure. Our results suggest that the compression behavior of liquid Sn changes from localized densification only in one cluster below ~ 3 GPa to homogeneous structural changes in both clusters above ~ 3 GPa.

ARTICLE HISTORY

Received 15 December 2014

Accepted 29 April 2016

KEYWORDS

Liquid Sn; high pressure; structure; hard sphere model

1. Introduction

Liquid Sn represents one typical liquid structure among three types of liquid metals.[1] The so-called Sn-type liquid metal possesses the structural characteristics, including: (i) a hump in the structure factor, $S(Q)$, as a shoulder at the high- Q side of the first diffraction peak, and (ii) ratio of the first (Q_1) and second (Q_2) peak positions of the $S(Q)$ (Q_2/Q_1 ratio) larger than a typical value (1.86) of most ($>80\%$) elemental liquid metals such as liquid Al. Several models have been proposed to explain the shoulder of Sn-type liquid. Orton [2,3] suggested a double hard sphere model by using two kinds of neighbor atoms which have different diameters with an approximation that the interaction between two different kinds of atoms is the same as the interaction of larger atom. Gabathuler and Steeb [4] proposed a similar model but contains hard spheres and tetrahedral units, instead of two sizes of hard spheres in Orton's model.[2,3] Canessa et al. [5] proposed a cluster model based on the concept that the Sn-type liquid consists of two types of clusters with two different kinds of hard spheres. Zou et al. [6,7] derived formulations based on Orton's [2,3] and Canessa et al.'s [5] concepts and reproduced experimental structural data.

Petkov and Yunchov [8] assumed that the local atomic ordering in liquid is similar to that in crystalline phase and applied the reverse Monte-Carlo simulation with diamond-type and β -Sn crystalline structure model. Munejiri et al. [9] performed molecular-dynamics simulation using distorted tetragonal units supposed to crystalline structure of β -Sn and bct structure instead of cubic units in diamond-type crystalline structures. Similarly, Narushima et al. [10] analyzed local structure of liquid Sn by applying a distorted-crystalline model using two crystalline structures of β -Sn and bct structure. Although the assumptions are different among these models, one common view is the anisotropic local structure in liquid Sn composed by two or more different unit structures, which is considered to be responsible for the hump at high- Q side of the first diffraction peak.

Effect of temperature on the structure of liquid Sn has been studied in several previous studies at ambient pressure.[1,4,7,11–14] These studies showed that the height of the hump decreases with increasing temperature. Yet it is still noticeable up to 1873 K. The Q_2/Q_1 ratio in $S(Q)$ weakly increases with increasing temperature. These data imply that liquid Sn keeps the anisotropic local structure at high temperatures up to 1873 K at ambient pressure. In addition, some efforts have been made to understand the structure of liquid Sn at high pressures.[10,15,16] Narushima et al. [10] studied the structure of liquid Sn up to 19.4 GPa along the melting curve, and observed a kink in the area of hump and the Q_2/Q_1 ratio around 3–6 GPa. They suggested that the structure of liquid Sn slightly changes toward simple liquid metal at low pressures (below 3–6 GPa). Then the trend stops at around 3–6 GPa, leading to an anisotropic structure in liquid Sn up to 19.4 GPa. However, since these high pressure experiments were conducted along melting curve, their observed structural changes are mixed by both pressure and temperature.

In this study, we have carried out high pressure experiments for liquid Sn at two isothermal conditions at 850 K up to 4.6 GPa and at 1373 K up to 5.3 GPa, in order to understand the effect of pressure and temperature separately on the structure of liquid Sn. The obtained structure factor, $S(Q)$, is fitted into a hard sphere cluster model (HSCM) [6,7] to indicate the changes of structural parameters at high pressure and high temperature conditions.

2. Experimental methods

The structure of liquid Sn was measured by *in situ* energy-dispersive X-ray diffraction (EDXD) at high pressures and high temperatures using a Paris–Edinburgh (PE) press at the 16-BM-B station at High Pressure Collaborative Access Team (HPCAT) at the Advanced Photon Source. We used a standard PE press assembly reported by Kono et al.[17] Temperatures were estimated using the power–temperature curves determined in a separate experiment using an identical cell assembly.[17] Errors in temperature are estimated to be less than 50 K by verifying the reproducibility of melting curves of NaCl and KCl.[18] Pressures are determined by the equation of state of MgO.[19] Pressure measurements were conducted before and after each structural measurement, and the difference in pressure was found to be less than 0.5 GPa.

Figure 1 shows the experimental pressure and temperature conditions in this study. Run-1 was conducted at four temperatures of 550, 650, 750 and 850 K around 1 GPa and then under isothermal compression at six pressures of 0.8, 1.6, 3.2, 4.0, 4.2 and 4.6 GPa at 850 K. In Run-2, the experiment was conducted at 10 temperatures of 573, 623,

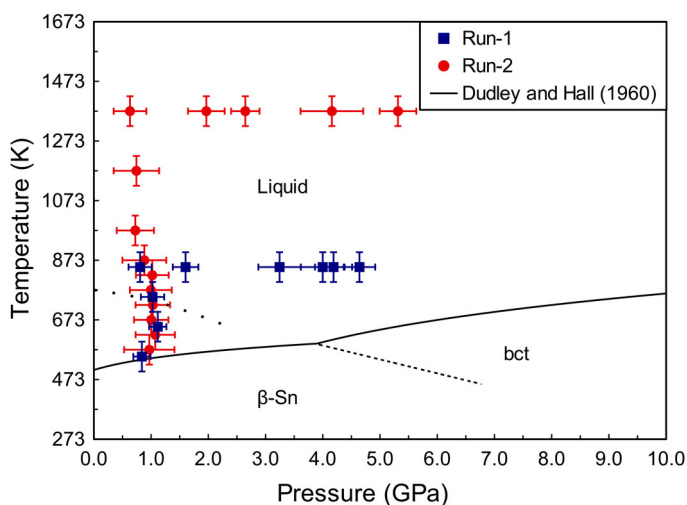


Figure 1. (Colour online) Experimental pressure–temperature conditions with the phase diagram of Sn. Blue squares and red circles show pressure and temperature conditions of Run-1 and Run-2, respectively. Errors in pressure are estimated to be less than 0.7 GPa that contains the differences of pressure between before and after a structural measurement about 0.4 GPa and errors in pressure calculation of about 0.2 GPa. Solid line represents melting curve.[33] Dashed line stands for the phase boundary between β -Sn and bct structure in crystalline Sn.[34] Dotted line shows the boundary of the liquid–liquid phase transition proposed by Brazhkin et al.[27]

673, 723, 773, 823, 873, 973, 1173 and 1373 K around 1 GPa, followed by isothermal compression at five pressures of 0.6, 2.0, 2.6, 4.2 and 5.3 GPa at 1373 K.

The structure factor $S(Q)$ of liquid Sn was measured by multi-angle EDXD using a Ge solid-state detector. EDXD patterns were collected at seven different diffraction angles ($2\theta = 3.0^\circ, 4.5^\circ, 6.0^\circ, 9.0^\circ, 12.0^\circ, 18.0^\circ$ and 25.0°). EDXD measurement at each angle was conducted with different time durations varying from 15 to 40 min, until the count has reached at least 1000 at 80 keV. Total data-acquisition time to complete the seven EDXD patterns was ~ 4 h. Background patterns at each 2θ angle were taken with the same experimental condition but using a cell assembly consisting of the same cell parts without sample.

Figure 2(a) shows EDXD patterns at the highest pressure and temperature condition (5.3 GPa and 1373 K) after background subtraction, with data binning to increase signal-to-noise ratio, and subtraction of crystalline peaks arising from the surrounding capsule material (BN) particularly at low 2θ angles. The absorption at ~ 69 keV is tungsten absorption edge from beamline components such as tungsten slits. The structure factors were analyzed using aEDXD, a program developed by Dr Changyong Park.[17] Figure 2(b) shows an example of the structure factor with a Q -coverage up to 15 \AA^{-1} , obtained by analyzing EDXD patterns shown in Figure 2(a). The Kaplow-type correction [20] and an optimization method described by Shen et al. [21] were applied in data analysis for $S(Q)$ (Figure 2 (c)). Typically, five iterations in optimization give reasonable converging results. We adopted the number density calculated by the second-order Birch–Murnaghan equation of state using the parameters reported in previous studies; a density ($\rho_0 = 6.979 \text{ g/cm}^3$ [22]) was used at the reference temperature (505.08 K [23]). Thermal expansion coefficient

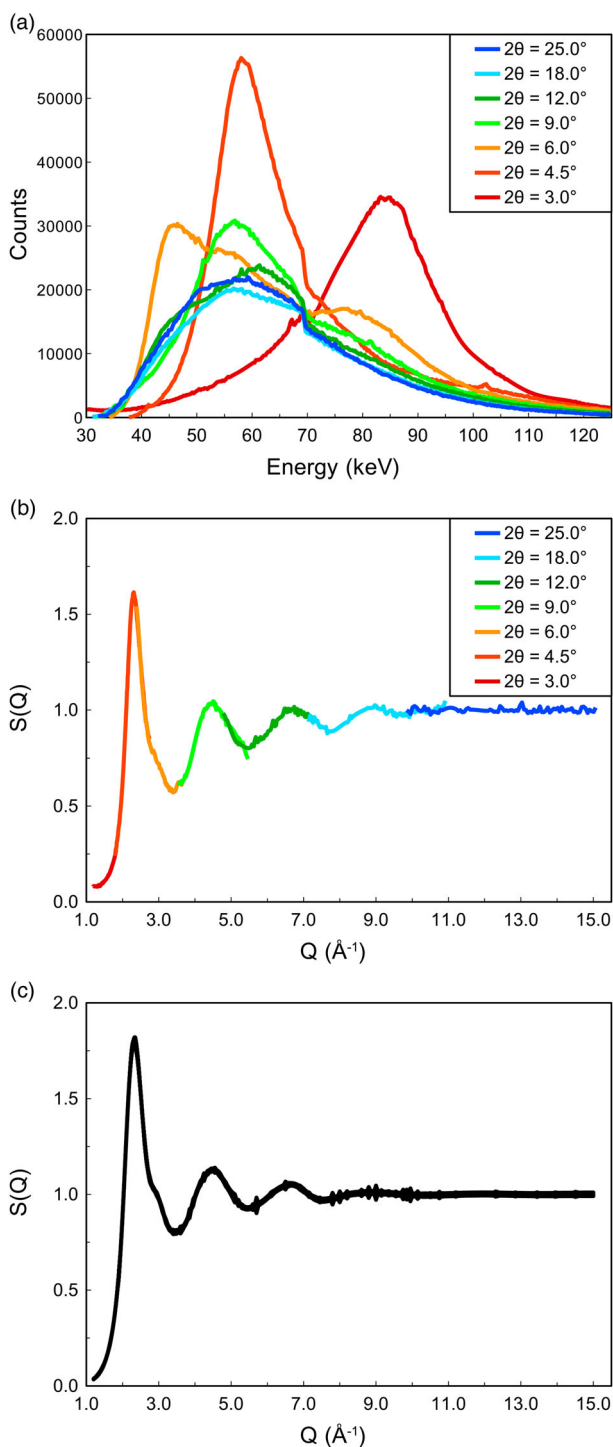


Figure 2. (Colour online) (a) EDXD patterns at seven 2θ angles at 5.3 GPa and 1373 K after background subtraction, data binning, and subtraction of crystalline peaks from the surrounding capsule material (BN). (b) An example of structure factor $S(Q)$ directly derived from the EDXD spectrums in (a). (c) The $S(Q)$ after optimization with the Kaplow correction.[20] Errors are indicated by the width of the line.

parameter α is $8.6 \times 10^{-5} \text{ (K}^{-1}\text{)}$ [24]. Isothermal bulk modulus ($K_{T(0)} = 38.12 \pm 7.86 \text{ GPa}$) and temperature dependence of bulk modulus ($dK_T/dT = -0.0146 \text{ GPa/K}$) are calculated from bulk sound velocity V_ϕ at high temperatures [25] using the density ρ [22] and thermal expansion coefficient parameter α [24] and Grüneisen parameter γ . [24]

$G(r)$ is then derived from the obtained $S(Q)$ as

$$G(r) = \frac{2}{\pi} \int_{Q_{\min}}^{Q_{\max}} Q[S(Q) - 1] \sin(Qr)L(Q)dQ \quad (1)$$

with the Lorch modified function $L(Q)$ [26]:

$$L(Q) = \frac{\sin(\pi Q/Q_{\max})}{\pi Q/Q_{\max}}. \quad (2)$$

3. Results

Figure 3 shows $S(Q)$ (Figure 3(a)–(b)) and $G(r)$ (Figure 3(c)–(d)) of liquid Sn with varying temperatures up to 1373 K at $\sim 1 \text{ GPa}$. The $S(Q)$ data show a hump on high- Q side of the first peak of the $S(Q)$, which is considered to reflect the anisotropic structure of liquid Sn.[3–10] The hump is relatively strong at low temperatures, and it becomes

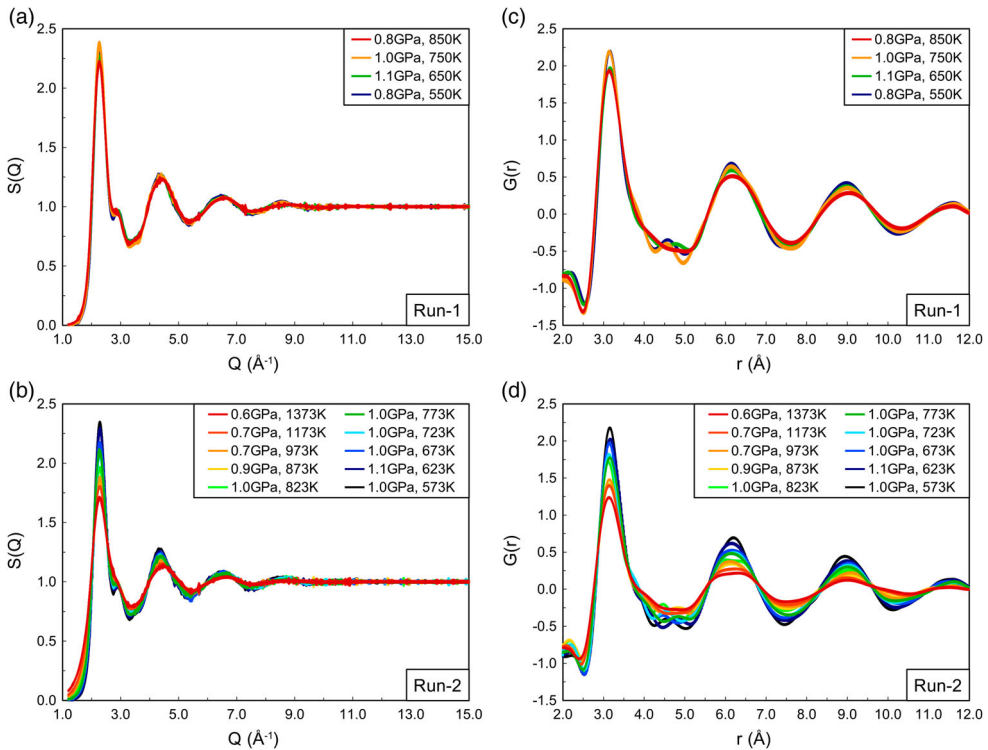


Figure 3. (Colour online) Structure factors $S(Q)$ and atomic pair distribution function $G(r)$ of liquid Sn with varying temperature. (a) and (b) show $S(Q)$ obtained in Run-1 and Run-2, respectively. (c) and (d) show $G(r)$ obtained in Run-1 and Run-2, respectively. The width of the line represents the errors.

broad and weak with increasing temperature. Figure 4 shows the temperature dependences of the height of (a) the first peak (Q_1) of $S(Q)$, (b) position of the Q_1 , (c) second peak (Q_2) position, (d) the Q_2/Q_1 ratio, (e) area of the hump, (f) the first peak (r_1) position of $G(r)$, (g) the second peak (r_2) position of $G(r)$ and (h) the r_2/r_1 ratio, with the numerical data summarized in Table 1. The area of the hump is determined by using the same method as described in [10]. The height of Q_1 decreases with increasing temperature. The Q_1 position is almost constant within errors up to the highest temperature (1373 K), while the Q_2 position linearly increases with increasing temperature. As a result, the Q_2/Q_1 ratio increases with increasing temperature. The area of the hump decreases with increasing temperature, yet the hump is still visible at the highest temperature of this study (1373 K). The area of hump at 1373 K is around 50% of that at the lowest temperature (550 K). The r_1 position decreases with increasing temperature, while the r_2 position is almost constant within errors up to 1373 K. The r_2/r_1 ratio increases gradually with increasing temperature.

Figure 5 shows $S(Q)$ and $G(r)$ of liquid Sn under isothermal compressions at 850 K (Figure 5(a) and 5(c)) and 1373 K (Figure 5(b) and 5(d)), respectively. Figure 6 shows the pressure dependences of the height of the Q_1 (a), Q_1 position (b), Q_2 position (c), the Q_2/Q_1 ratio (d), area of hump (e), r_1 position (f), r_2 position (g) and the r_2/r_1 ratio (h), with their numerical data summarized in Table 1. We observed almost linear change in peak positions and their ratios with varying pressure. Q_1 and Q_2 positions show gradual increase with increasing pressure (Figure 5(b) and 5(c)), and the Q_2/Q_1 ratio decreases gradually with increasing pressure (Figure 5(d)). The Q_2/Q_1 ratio is still larger than 1.86, a typical value of simple liquid metals,[1] even at the highest pressure of 5.3 GPa. The area of hump is almost constant between 0.6 and 5.3 GPa at both temperature conditions of 850 and 1373 K (Figure 5e). r_1 , r_2 position and the r_2/r_1 ratio gradually decreases with increasing pressure (Figure 5(f)–(h)). In contrast, we find a turn-over in the pressure dependence of the height of Q_1 (Figure 5(a)). The height of Q_1 increases with increasing pressure below around 3 GPa, while it begins to decrease at pressures higher than ~ 3 GPa. We observed similar behavior in the height of Q_1 at both 850 and 1373 K, while the degree of change is larger at 850 K than that at 1373 K.

4. Discussion

Our data show gradual change in height and peak positions of the $S(Q)$ and $G(r)$ with varying temperature at ~ 1 GPa. Our obtained temperature dependence of the area of hump and the Q_2/Q_1 ratio at ~ 1 GPa are similar to those at ambient pressure reported in previous studies.[1,4,11–14] A previous study by Brazhkin et al. [27] proposed liquid–liquid phase transition at ~ 0 –3 GPa at ~ 773 –673 K (Figure 1) from an experimental results of discontinuous volume change. However, our data show no obvious structural change around 723 K at 1 GPa, which is consistent with some recent studies.[10,28]

On the other hand, we find a turn-over in the pressure dependence of the height of Q_1 at ~ 3 GPa. Similarly, Narushima et al. [10] have reported a kink in the pressure dependence of the area of hump, the Q_2/Q_1 ratio and r_2/r_1 ratio at ~ 3 –6 GPa along melting curve (~ 573 –673 K). Although our results show no clear kink in the pressure dependence of the area of hump (Figure 6(e)), the Q_2/Q_1 ratio (Figure 6(d)), and the r_2/r_1 ratio (Figure 6(h)), possibly due to limited pressure range of our experiments up to 5.3 GPa, distinct

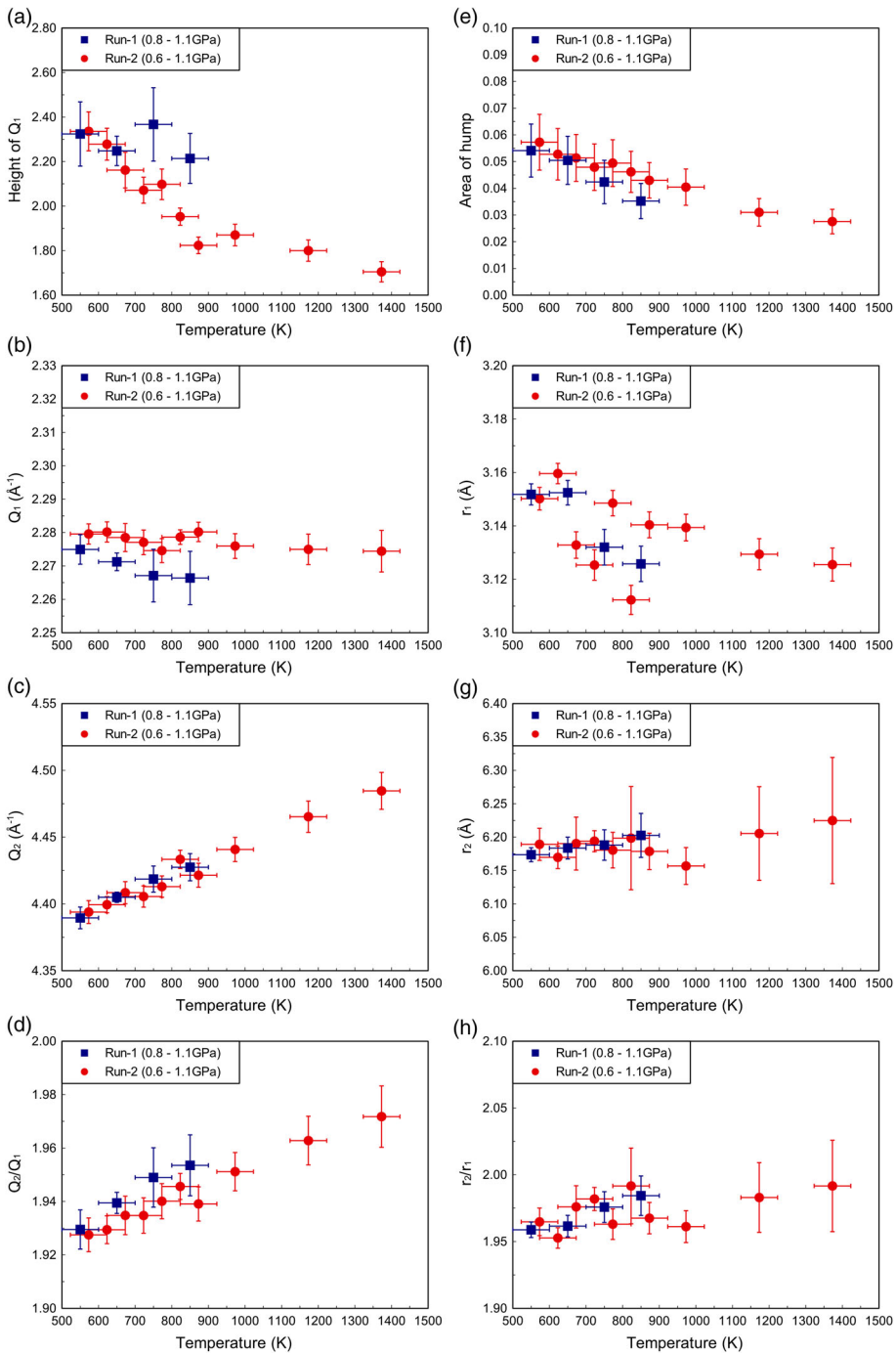


Figure 4. (Colour online) Temperature dependence of the height of (a) the first peak position in $S(Q)$, (b) first peak (Q_1) position in $S(Q)$, (c) second peak (Q_2) position in $S(Q)$, (d) the Q_2/Q_1 ratio – which is the ratio of the positions of the first (Q_1) and second (Q_2) diffraction peaks in $S(Q)$, (e) area of hump, (f) first peak (r_1) position in $G(r)$, (g) second peak (r_2) position in $G(r)$ and (h) the r_2/r_1 ratio, which is the ratio of the positions of the first (r_1) and second (r_2) diffraction peaks in $G(r)$ of liquid Sn. The area of hump is determined by the same method as that of Narushima et al.[10]

Table 1. Structural information of liquid Sn at high temperatures and high pressures.

Run	P (GPa)	T (K)	Height of Q_1	Q_1 (\AA^{-1})	Q_2 (\AA^{-1})	Q_2/Q_1	Area of hump	r_1 (\AA)	r_2 (\AA)	r_2/r_1
1	0.8(2)	550	2.32(14)	2.275(4)	4.390(8)	1.930(7)	0.054(10)	3.152(4)	6.174(11)	1.959(6)
1	1.1(2)	650	2.25(7)	2.271(3)	4.405(4)	1.939(4)	0.050(9)	3.152(5)	6.184(16)	1.962(8)
1	1.0(2)	750	2.37(16)	2.267(8)	4.419(10)	1.949(11)	0.042(8)	3.132(7)	6.188(23)	1.976(12)
1	0.8(2)	850	2.21(11)	2.266(8)	4.427(10)	1.954(11)	0.035(7)	3.126(7)	6.203(33)	1.984(15)
1	1.6(2)	850	2.44(3)	2.277(2)	4.440(6)	1.950(4)	0.038(7)	3.118(7)	6.167(32)	1.978(15)
1	3.2(4)	850	2.51(7)	2.296(6)	4.445(9)	1.936(9)	0.039(7)	3.106(6)	6.107(21)	1.966(11)
1	4.0(4)	850	2.30(6)	2.305(4)	4.462(9)	1.936(7)	0.043(8)	3.095(6)	6.065(34)	1.959(15)
1	4.2(3)	850	2.26(7)	2.311(5)	4.460(10)	1.929(9)	0.044(8)	3.086(6)	6.059(37)	1.963(16)
1	4.6(3)	850	2.29(11)	2.317(7)	4.462(10)	1.926(10)	0.043(8)	3.097(4)	6.054(22)	1.955(10)
2	1.0(4)	573	2.34(9)	2.280(3)	4.394(9)	1.928(6)	0.057(10)	3.150(4)	6.189(24)	1.965(10)
2	1.1(3)	623	2.28(7)	2.280(3)	4.399(6)	1.929(5)	0.053(10)	3.160(4)	6.170(17)	1.953(8)
2	1.0(3)	673	2.16(8)	2.279(4)	4.408(8)	1.935(7)	0.051(9)	3.133(5)	6.190(40)	1.976(16)
2	1.0(3)	723	2.07(6)	2.277(4)	4.406(8)	1.935(7)	0.048(9)	3.125(6)	6.194(16)	1.982(9)
2	1.0(4)	773	2.10(7)	2.275(4)	4.413(8)	1.940(7)	0.049(9)	3.149(5)	6.181(27)	1.963(11)
2	1.0(3)	823	1.95(4)	2.279(2)	4.433(7)	1.946(5)	0.046(8)	3.112(5)	6.198(77)	1.992(28)
2	0.9(4)	873	1.82(4)	2.280(3)	4.421(9)	1.939(6)	0.043(7)	3.140(5)	6.179(27)	1.967(12)
2	0.7(3)	973	1.87(5)	2.276(4)	4.441(9)	1.951(7)	0.040(7)	3.139(5)	6.157(28)	1.961(12)
2	0.7(4)	1173	1.80(5)	2.275(5)	4.465(12)	1.963(9)	0.031(5)	3.129(6)	6.205(70)	1.983(26)
2	0.6(3)	1373	1.70(5)	2.274(6)	4.485(14)	1.972(11)	0.028(5)	3.126(6)	6.225(94)	1.992(34)
2	2.0(3)	1373	1.77(5)	2.288(5)	4.502(12)	1.968(10)	0.029(4)	3.116(6)	6.168(56)	1.980(22)
2	2.6(3)	1373	1.84(6)	2.296(6)	4.504(13)	1.962(11)	0.032(5)	3.112(6)	6.126(34)	1.969(15)
2	4.2(6)	1373	1.85(5)	2.309(4)	4.500(12)	1.949(9)	0.037(6)	3.107(5)	6.097(37)	1.962(15)
2	5.3(3)	1373	1.80(5)	2.321(4)	4.503(12)	1.940(9)	0.036(6)	3.103(5)	6.055(44)	1.951(17)

Note: Q_1 = first peak position of $S(Q)$, Q_2 = second peak position of $S(Q)$, Q_2/Q_1 = ratio of the first and second peak of $G(r)$, r_1 = first peak position of $G(r)$, r_2 = first peak position of $G(r)$, r_2/r_1 = ratio of the first and second peak of $G(r)$.

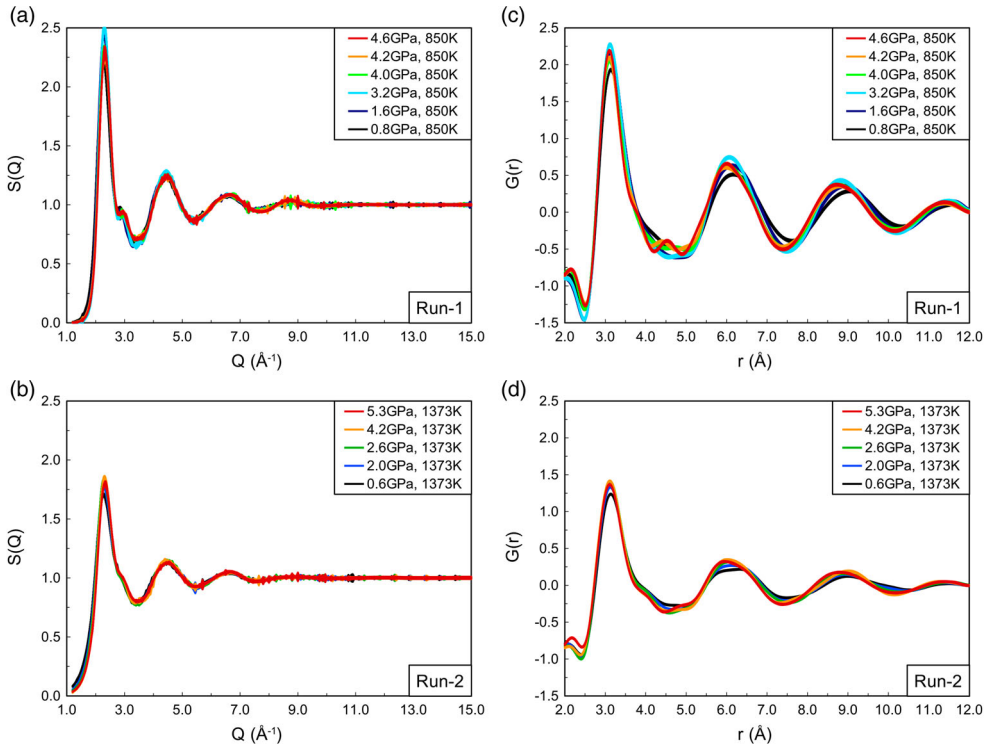


Figure 5. (Colour online) Structure factors $S(Q)$ and atomic pair distribution function $G(r)$ of liquid Sn with varying pressure at two temperature conditions (850 K and 1373 K). (a) and (b) show $S(Q)$ obtained in Run-1 and Run-2, respectively. (c) and (d) show $G(r)$ obtained in Run-1 and Run-2, respectively. The width of the line represents the errors.

turn-over in the height of Q_1 at ~ 3 GPa under both 850 and 1373 K imply existence of pressure-induced change in compression behavior of liquid Sn at around 3 GPa.

Hard sphere model has been widely used to describe the structure of liquid metals.[1] In hard sphere system, undeformable hard spheres are assumed to have been filled with random irregularities and without overlapping. This filling theory was proposed by Ornstein and Zernike [29] and has been used with some additional approximation such as Percus–Yevick [30] approximation.

Ashcroft and Lekner [31] obtained the structure factor $S(Q)$ in the hard sphere model of single component system that is expressed by the following equations:

$$S(Q\sigma) = \frac{1}{\rho_N f(Q\sigma)}, \quad (3)$$

$$f(Q\sigma) = 4\pi\sigma^3 \int_0^1 s^2 \frac{\sin(sQ\sigma)}{sQ\sigma} (A + Bs + Cs^3) ds, \quad (4)$$

$$A = \frac{(1 + 2\eta)^2}{(1 - 4\eta)^4}, \quad B = -6\eta \frac{(1 + \eta/2)^2}{(1 - \eta)^4}, \quad C = \frac{\eta(1 + 2\eta)^2}{2(1 - 4\eta)^4}, \quad (5)$$

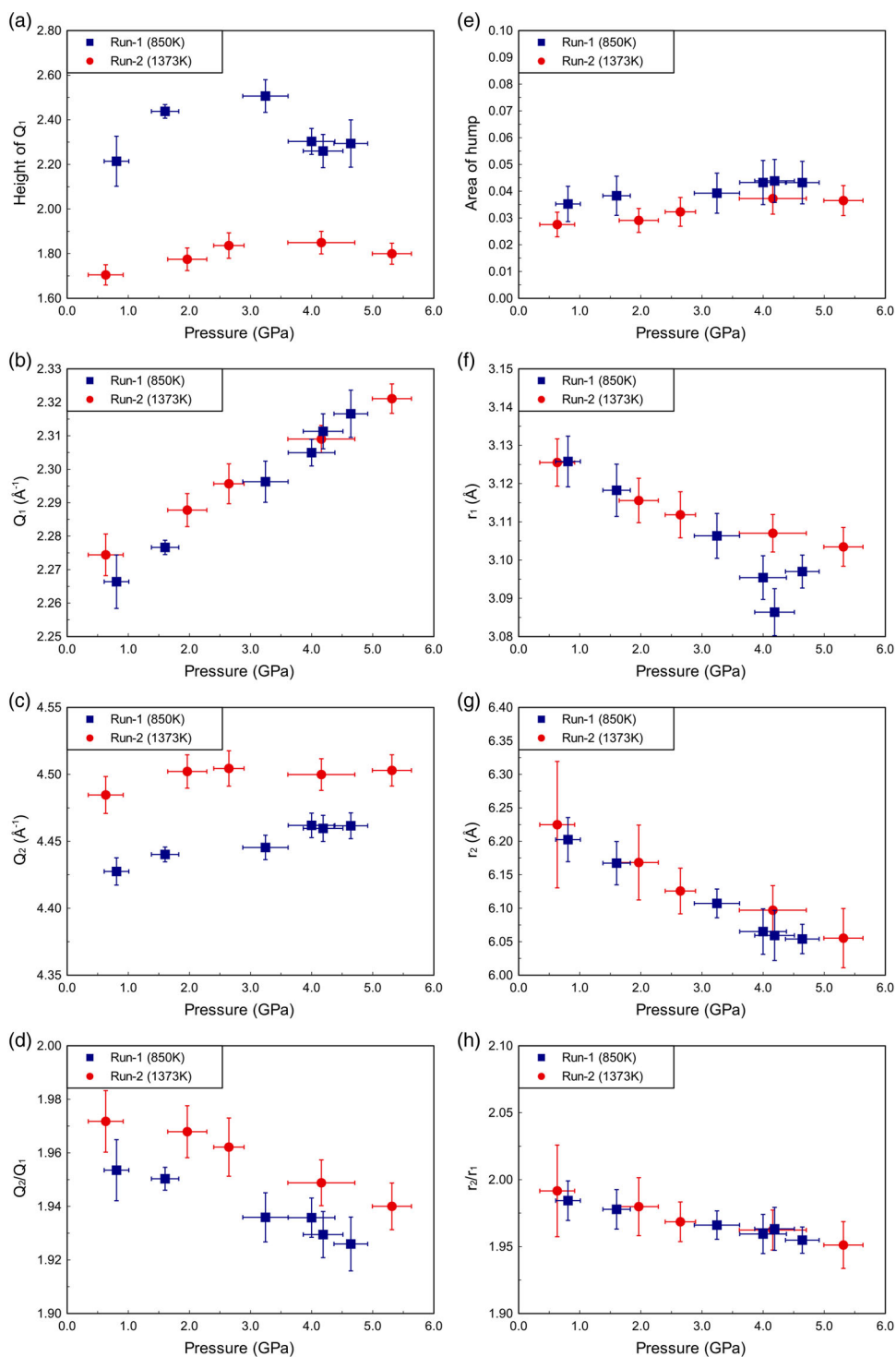


Figure 6. (Colour online) Pressure dependence of the height of (a) the first peak position in $S(Q)$, (b) first peak (Q_1) position in $S(Q)$, (c) second peak (Q_2) position in $S(Q)$, (d) the Q_2/Q_1 ratio, (e) area of hump, (f) first peak (r_1) position in $G(r)$, (g) second peak (r_2) position in $G(r)$ and (h) the r_2/r_1 ratio.

$$\rho_N = \frac{6\eta}{\pi\sigma^3}, \quad (6)$$

where η is the packing fraction; σ is the hard sphere diameter. Number density (ρ_N) is correlated with packing fraction and hard sphere diameter (Equation (6)), and therefore the hard sphere model of single component system is defined by two free parameters. Previous studies noted that the single component model can well simulate $S(Q)$ of simple Al-type liquid metals. However, it is difficult to simulate Sn-type liquid metals by the single component hard sphere model.[1]

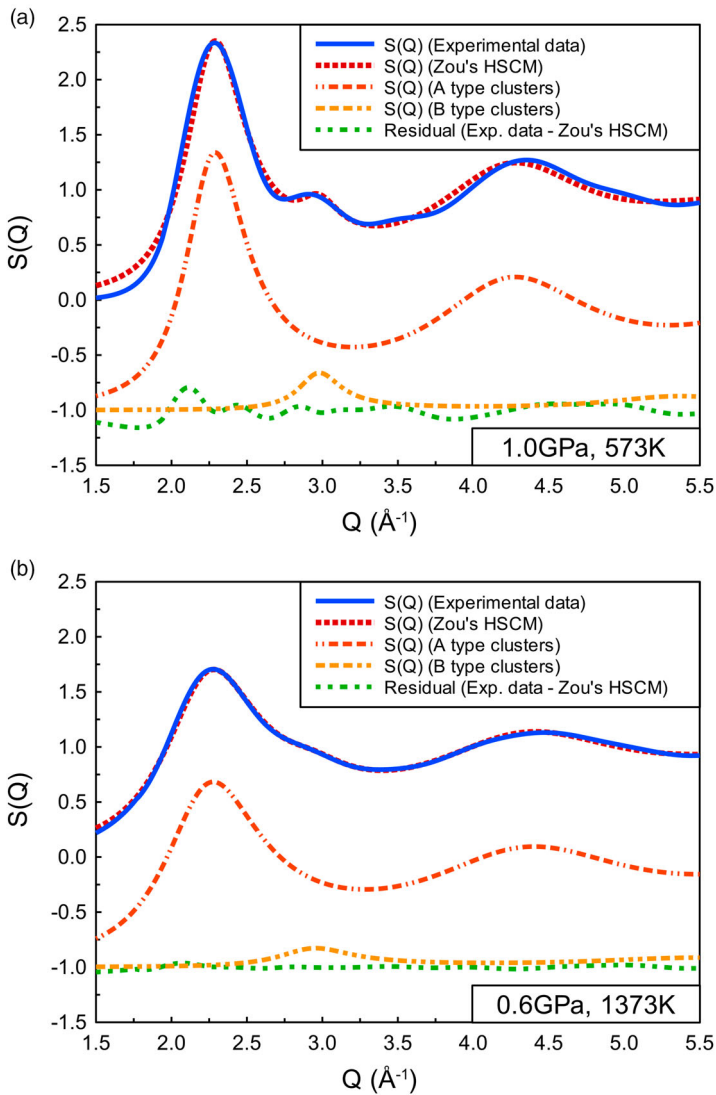


Figure 7. (Colour online) Examples of the fitting of $S(Q)$ using Zou's HSCM.[6,7] The $S(Q)$ patterns of A- and B-type clusters and the residual between experimental data and Zou's HSCM are shown by offset of -1 in vertical axis.

We used Zou's HSCM [6,7] to fit $S(Q)$ of liquid Sn. In Zou's model, Sn-type liquid metal is assumed as a mixture of two types of clusters (A- and B-type atoms), and the total structure factor is described as a summation of weighted partial $S(Q)$ of the two type of clusters [6,7]:

$$S_{\text{total}}(Q) = x_A S_A(Q) + (1 - x_A) S_B(Q), \quad (7)$$

where x_A is the fraction of A-type atoms, and $S_i(Q)$ is the structure factor of i -type clusters which can be expressed as the same as a single component hard sphere model (Equations (3)–(6)). Each $S_i(Q)$ has been defined by two free parameters of η_i (the packing fraction) and σ_i (the hard sphere diameter). Thus, $S(Q)$ in Zou's HSCM is obtained

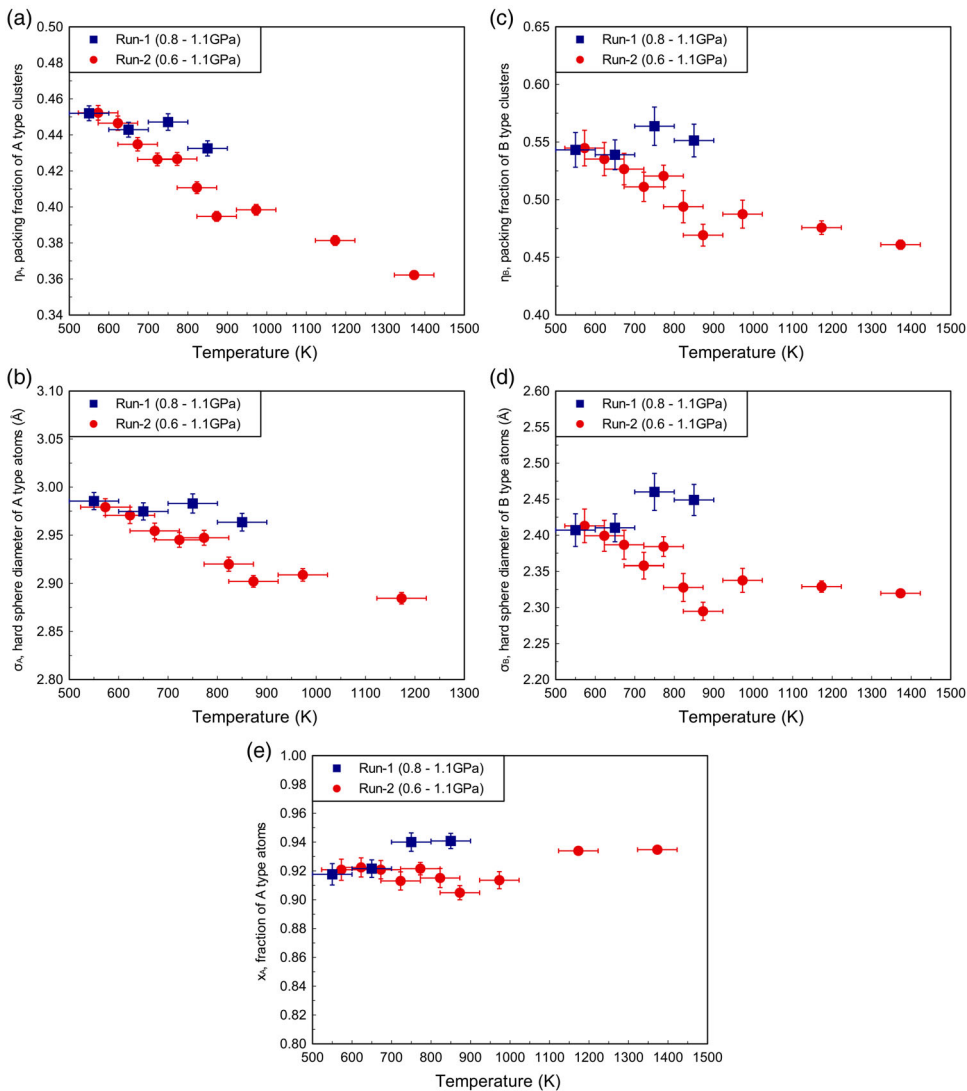


Figure 8. (Colour online) Temperature dependence of packing fraction, hard sphere diameter and fraction of A-type atoms obtained by fitting into Zou's HSCM. (a) and (c) show temperature dependence of the packing fraction of A- and B-type clusters, respectively. (b) and (d) show temperature dependence of the hard sphere diameter of A- and B-type atoms, respectively. (e) shows temperature dependence of the fraction of A-type atoms.

Table 2. Parameters used in Zou's HSCM for fitting the structure factors of liquid Sn at high temperatures and high pressures.

Run	P (GPa)	T (K)	η_A	σ_A (Å)	η_B	σ_B (Å)	x_A
1	0.8(2)	550	0.452(4)	2.985(9)	0.543(15)	2.407(23)	0.918(7)
1	1.1(2)	650	0.443(4)	2.975(9)	0.539(13)	2.410(19)	0.922(6)
1	1.0(2)	750	0.447(5)	2.983(10)	0.564(17)	2.460(26)	0.940(6)
1	0.8(2)	850	0.433(4)	2.963(9)	0.551(14)	2.449(22)	0.941(5)
1	1.6(2)	850	0.451(5)	2.975(11)	0.573(19)	2.472(30)	0.951(6)
1	3.2(4)	850	0.459(5)	2.962(10)	0.572(19)	2.438(30)	0.946(7)
1	4.0(4)	850	0.446(4)	2.934(9)	0.532(14)	2.350(21)	0.928(6)
1	4.2(3)	850	0.444(4)	2.926(9)	0.527(14)	2.343(20)	0.924(6)
1	4.6(3)	850	0.449(4)	2.925(9)	0.531(13)	2.344(19)	0.924(6)
2	1.0(4)	573	0.452(4)	2.979(9)	0.545(15)	2.413(23)	0.921(7)
2	1.1(3)	623	0.447(4)	2.971(9)	0.535(14)	2.399(22)	0.922(7)
2	1.0(3)	673	0.435(4)	2.954(8)	0.527(14)	2.387(20)	0.921(6)
2	1.0(3)	723	0.426(4)	2.945(8)	0.511(13)	2.358(18)	0.913(6)
2	1.0(4)	773	0.427(4)	2.947(8)	0.521(9)	2.384(14)	0.922(4)
2	1.0(3)	823	0.411(3)	2.920(7)	0.494(14)	2.328(19)	0.915(7)
2	0.9(4)	873	0.395(3)	2.902(6)	0.469(9)	2.295(13)	0.905(5)
2	0.7(3)	973	0.398(3)	2.909(7)	0.487(12)	2.338(17)	0.914(6)
2	0.7(4)	1173	0.381(3)	2.885(6)	0.476(6)	2.329(8)	0.934(2)
2	0.6(3)	1373	0.362(2)	2.862(5)	0.461(4)	2.320(5)	0.935(1)
2	2.0(3)	1373	0.377(3)	2.864(6)	0.466(6)	2.292(8)	0.928(2)
2	2.6(3)	1373	0.387(3)	2.868(6)	0.473(6)	2.296(8)	0.926(3)
2	4.2(6)	1373	0.396(3)	2.866(7)	0.454(13)	2.270(16)	0.901(7)
2	5.3(3)	1373	0.394(3)	2.853(6)	0.428(7)	2.210(8)	0.881(4)

Note: η_A = packing fraction of A-type clusters, σ_A = hard sphere diameter of A-type atoms (Å), η_B = packing fraction of B-type clusters, σ_B = hard sphere diameter of B-type atoms (Å), x_A = fraction of A-type atoms.

by five free parameters (x_A , η_A , η_B , σ_A , σ_B). The Zou's equation is consistent with a model for binary alloys by Wagner and Halder [32] when the interference function between different type of atoms ($S_{AB}(Q)$) is $2S_{AB}(Q) = S_A(Q) + S_B(Q)$. Figure 7 shows typical fitting results of $S(Q)$ compared with the fitting results by Zou's HSCM. Both fitting results agree well with experimentally obtained $S(Q)$ at 0.9 GPa and 1073 K (a) and 6.9 GPa and 1773 K (b). The B-type atom cluster mainly constitute the hump while it shows small contribution to peak positions and heights of Q_1 and Q_2 .

Figure 8 shows the temperature dependence of the packing fraction of (a) A-type clusters (η_A), (b) the hard sphere diameter (Å) of A-type atoms (σ_A), (c) the packing fraction of B-type clusters (η_B), (d) the hard sphere diameter (Å) of B-type atoms (σ_B), (e) the fraction of A-type atoms (x_A), with the numerical data summarized in Table 2. The packing fractions of A-type and B-type clusters decrease $\sim 20\%$ and $\sim 15\%$ with increasing temperature from 573 to 1373 K, respectively (Figure 8(a) and 8(c)). The hard sphere diameters of both A-type and B-type atoms also decrease $\sim 4\%$ with increasing temperature from 573 to 1373 K (Figure 8(b) and 8(d)). The temperature dependence of packing fraction and hard sphere diameter of each cluster is similar to those of simple liquid metals such as liquid Al.[1] Fraction of A-type atoms is almost constant around 0.92–0.94 within 2% error up to 1373 K (Figure 8(e)). These data suggest that the liquid Sn remains an anisotropic structure with varying temperature, and that the behavior of each cluster in liquid Sn is similar to that of simple liquid metal such as liquid Al.[1]

Figure 9 shows the pressure dependence of the packing fraction of (a) A-type clusters (η_A), (b) the hard sphere diameter (Å) of A-type atoms (σ_A), (c) the packing fraction of B-type clusters (η_B), (d) the hard sphere diameter (Å) of B-type atoms (σ_B), (e) the fraction of A-type atoms (x_A), with the numerical data summarized in Table 2. The packing fraction

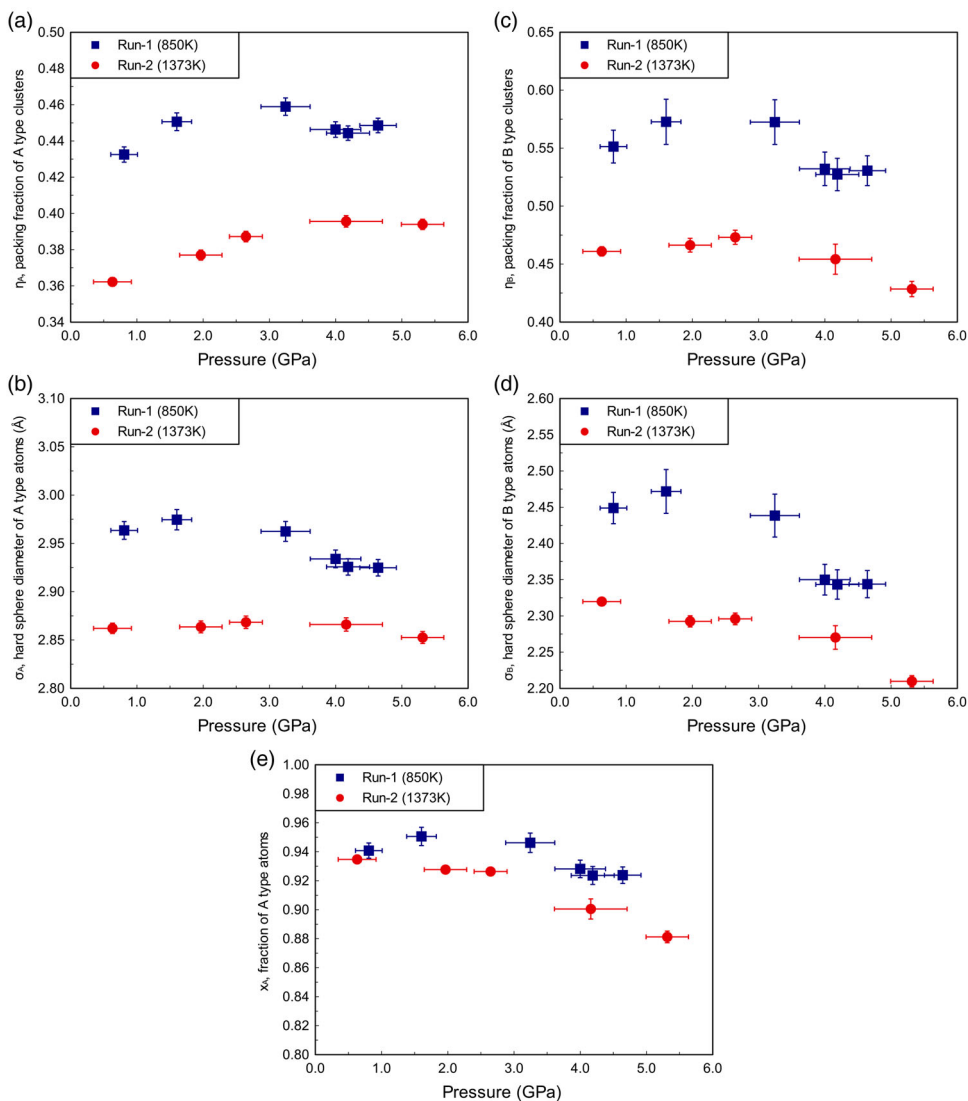


Figure 9. (Colour online) Pressure dependence of packing fraction, hard sphere diameter and fraction of A-type atoms obtained by fitting into Zou's HSCM. (a) and (c) show pressure dependence of the packing fraction of A- and B-type clusters, respectively. (b) and (d) show pressure dependence of the hard sphere diameter of A- and B-type atoms, respectively. (e) shows pressure dependence of the fraction of A-type atoms.

of A-type cluster increases with increasing pressure up to around 3 GPa; it then turns over and starts decreasing above ~ 3 GPa (Figure 9(a)). On the other hand, the packing fraction of B-type clusters is almost constant below ~ 3 GPa, while it decreases above ~ 3 GPa (Figure 9(c)). Hard sphere diameters of both A and B types are almost constant below 3 GPa, and then they decrease above ~ 3 GPa (Figure 9(b) and 9(d)). Fraction of A-type atoms is almost constant below ~ 3 GPa, while it slightly decreases with increasing pressure above ~ 3 GPa (Figure 9(e)).

These results suggest that the compression behavior of liquid Sn changes around 3 GPa. Below ~ 3 GPa, only the packing fraction of A-type cluster changes by compression without any changes in B-type cluster (Figure 9(c) and 9(d)). In contrast, above ~ 3 GPa, the packing fraction and the hard sphere diameter of both A- and B-type clusters decrease with increasing pressure (Figure 9). These data suggest that compression mechanism of liquid Sn changes from localized densification via reducing the packing fraction of A-type cluster below ~ 3 GPa to homogeneous structural changes in both A- and B-type clusters above ~ 3 GPa.

Acknowledgement

We acknowledge an anonymous reviewer for valuable comment. We thank Curtis Kenney-Benson for his help in PE cell experiment and Changyong Park for his help in the aEDXD program. This work was performed at HPCAT (Sector 16), Advanced Photon Source (APS), Argonne National Laboratory. The Advanced Photon Source is a US Department of Energy (DOE) Office of Science User Facility operated for the DOE Office of Science by Argonne National Laboratory under Contract No. DE-AC02-06CH11357.

Disclosure statement

No potential conflict of interest was reported by the authors.

Funding

This research is supported by DOE DE-FG02-99ER45775 and DE-NA0001974. HPCAT operations are supported by DOE-NNSA under Award No. DE-NA0001974 and DOE-BES under Award No. DE-FG02-99ER45775, with partial instrumentation funding by NSF. The PE cell program is partly supported by GeoSoilEnviroCARS (GSECARS), which is supported by the NSF-EAR (EAR-1128799) and DOE-GeoSciences (DE-FG02-94ER14466).

References

- [1] Waseda Y. The structure of non-crystalline materials: liquids and amorphous solids. New York: McGraw-Hill International Book Co; 1980.
- [2] Orton BR. A model of the structure of liquid germanium. *Z Naturforsch.* 1975;30a:1500–1502.
- [3] Orton BR. A double hard sphere model of liquid semi-metals: Applications to bismuth and tin. *Z Naturforsch.* 1979;34a:1547–1550.
- [4] Gabathuler JP, Steeb S. Structure of Si-Melts, Ge-Melts, Sn-Melts, and Pb-Melts. *Z Naturforsch.* 1979;34a:1314–1319.
- [5] Canessa E, Mariani DF, Vignolo J. Structure of non-simple liquid metals. *Phys Status Solidi B.* 1984 Aug;124:465–472.
- [6] Zou XW, Jin ZZ, Shang YJ. Static structure factor of non-simple liquid metals Bi, Ga, Sb, and Sn. *Phys Status Solidi B.* 1987 Feb;139:365–370.
- [7] Zou XW, Jin ZZ, Tang SQ. Temperature dependence of the static structure factor for liquid Bi, Ga, Sb, and Sn. *Phys Status Solidi B.* 1987 Jul;142:9–14.
- [8] Petkov V, Yunchov G. Atomic-scale structures of liquid Sn, Ge and Si by reverse Monte Carlo simulations. *J Phys Condens Matter.* 1994 Dec;6:10885–10895.
- [9] Munejiri S, Shimojo F, Hoshino K, Di Cicco A. Structure of liquid tin under high pressure by ab initio molecular-dynamics simulation. *J. Phys. Conf. Ser.* 2008 Feb;98:Article no. 42010. doi:10.1088/1742-6596/98/4/042010
- [10] Narushima T, Hattori T, Kinoshita T, Hinzmann A, Tsuji K. Pressure dependence of the structure of liquid Sn up to 19.4 GPa. *Phys Rev B.* 2007 Sep;76:Article no. 104204. doi:10.1103/PhysRevB.76.104204

- [11] Furukawa K, Orton BR, Hamor J, Williams GI. The structure of liquid tin. *Philos Mag.* 1963 Jan;8:141–155.
- [12] Takeda S, Tamaki S, Waseda Y. Neutron diffraction study of liquid Bi-Sn alloys. *J Phys Soc Jpn.* 1984 Oct;53:3447–3456.
- [13] Hosokawa S, Greif J, Demmel F, Pilgrim WC. Quasielastic lineshape of liquid Sn studied by inelastic X-ray scattering. *Chem Phys.* 2003 Aug;292:253–261.
- [14] Itami T, Munejiri S, Masaki T, Aoki H, Ishii Y, Kamiyama T, Senda Y, Shimojo F, Hoshino K. Structure of liquid Sn over a wide temperature range from neutron scattering experiments and first-principles molecular dynamics simulation: A comparison to liquid Pb. *Phys Rev B.* 2003 Feb;67:Article no. 064201. doi:10.1103/PhysRevB.67.064201
- [15] Katayama Y, Inamura Y. Synchrotron radiation studies on pressure-induced structural changes in liquids and glasses. *J Phys Condens Matter.* 2003 Jan;15:S343–S350.
- [16] Tsuji K, Hattori T, Mori T, Kinoshita N, Narushima T, Funamori N. Pressure dependence of the structure of liquid group 14 elements. *J Phys Condens Matter.* 2004 Apr;16:S989–S996.
- [17] Kono Y, Park C, Kenney-Benson C, Shen G, Wang Y. Toward comprehensive studies of liquids at high pressures and high temperatures: Combined structure, elastic wave velocity, and viscosity measurements in the Paris–Edinburgh cell. *Phys Earth Planet Inter.* 2014 Mar;228:269–280.
- [18] Kono Y, Kenney-Benson C, Park C, Shen G, Wang Y. Anomaly in the viscosity of liquid KCl at high pressures. *Phys Rev B.* 2013 Jan;87:Article no. 024302. doi:10.1103/PhysRevB.87.024302
- [19] Kono Y, Irifune T, Higo Y, Inoue T, Barnhoorn A. P-V-T relation of MgO derived by simultaneous elastic wave velocity and in situ X-ray measurements: A new pressure scale for the mantle transition region. *Phys. Earth Planet Inter.* 2010 Nov;183:196–211.
- [20] Kaplow R, Strong SL, Averbach BL. Radial density functions for liquid mercury and lead. *Phys Rev.* 1965 May;138:A1336–A1345.
- [21] Shen G, Prakupenka VB, Rivers ML, Sutton SR. Structural investigation of amorphous materials at high pressures using the diamond anvil cell. *Rev Sci Instrum.* 2003 Jun;74:3021–3026.
- [22] Assael MJ, Kalyva AE, Antoniadis KD, Banish RM, Egly I, Wu J, Kaschnitz E, Wakeham WA. Reference data for the density and viscosity of liquid copper and liquid tin. *J Phys Chem Ref Data.* 2010 Sep;39:Article no. 033105. doi:10.1063/1.3467496
- [23] Preston-Thomas H. The international temperature scale of 1990 (ITS-90). *Metrologia.* 1990 Jan;27:3–10.
- [24] Nasch PM, Steinemann SG. Density and thermal expansion of molten manganese, iron, nickel, copper, aluminum and tin by means of the gamma-ray attenuation technique. *Phys Chem Liq.* 1995 Jan;29:43–58.
- [25] Turner R, Crozier ED, Cochran JF. A new technique for measuring the velocity of sound in liquid metals. *Can J Phys.* 1972 Nov;50:2735–2740.
- [26] Lorch E. Neutron diffraction by germania, silica and radiation-damaged silica glasses. *J Phys C Solid State Phys.* 1969 Feb;2:229–237.
- [27] Brazhkin VV, Popova SV, Voloshin RN. High-pressure transformations in simple melts. *High Press Res.* 1997 Feb;15:267–305.
- [28] Di Cicco A, Trapananti A, Principi E, De Panfilis S, Filipponi A. Polymorphism and metastable phenomena in liquid tin under pressure. *Appl Phys Lett.* 2006 Nov;89:Article no. 221912. doi:10.1063/1.2397568
- [29] Ornstein LS, Zernike F. Accidental deviations of density and opalescence at the critical point of a single substance. *Proc K Akad Van Wet Te Amst.* 1914;17:793–806.
- [30] Percus JK, Yevick GJ. Analysis of classical statistical mechanics by means of collective coordinates. *Phys Rev.* 1958 Apr;110:1–13.
- [31] Ashcroft NW, Lekner J. Structure and resistivity of liquid metals. *Phys Rev.* 1966 May;145:83–90.
- [32] Wagner CNJ, Halder NC. Atomic distribution and electronic transport properties in liquid alloys studied by X-ray diffraction. *Adv Phys.* 1967 Apr;16:241–261.
- [33] Dudley JD, Hall HT. Experimental fusion curves of indium and tin to 105 000 atmospheres. *Phys Rev.* 1960 Jun;118:1211–1216.
- [34] Barnett JD, Bennion RB, Hall HT. X-ray diffraction studies on tin at high pressure and high temperature. *Science.* 1963 Sep;141:1041–1042.